ABSTRACT

In Quantum Chromodynamics (QCD), quarks and gluons are confined. The same theory, however predicts that at very high temperatures and/or densities, these particles behave as free particles. This state is called the Quark Gluon Plasma (QGP). ALICE is one of the four experiments at the Large Hadron Collider (LHC) in Geneve and it's main purpose is to study the properties of the QGP produced by colliding lead(Pb) ions at a center of mass energy of 2.76 TeV per nucleon. In this thesis we use data from this experiment from Pb-Pb collisions.

In this field, heavy quarks are excellent probes to study the QGP. This is for two main reasons. The first reason is the production time. The prodcution time is related to mass by $1/m_q$ and therefore heavy quarks are created early in the collision. Because of this heavy quarks are formed before the QGP is formed. The second reason is that heavy quarks lose less energy than lighter quarks so when they travel through QGP they can penetrate deeper.

The two quarks we are studying are the charm and the beauty quark. We will not be able to observe these quarks directly though, so we will look at charged mesons. Mesons consist of a quark and an anti-quark. The two mesons which will be the main focus in this thesis are the B^0, which contains a beauty quark, and the D^{*+}, which contains a charm quark.

This thesis is divided in two parts. The first part uses real data from Pb-Pb collisions in ALICE from 2011. From this data we can reconstruct the D^{*+}. We can not do the same for the B^0, because there is not enough data. That is why the second part uses Monte Carlo simulations, generated by the event generator PYTHIA. Currently, CERN is upgrading its accelerator to provide a center of mass energy of 13 TeV in p-p collisions (it is now 7 TeV in p-p and 5.5 TeV in Pb-Pb collisions). We will look at the prospects of finding the B^0 after the upgrade and study its properties.

Contents

1 Introduction

Since the mid-1970s, the Standard Model has functioned as an excellent tool in predicting and describing the properties of elementary particle physics. The theory has since then posed us with a lot of questions, of which many still remain. In an attempt to answer these questions physicists made use of particle accelerators, culminating in the Large Hadron Collider (LHC). The LHC was finished in 2008 and consists of a 27 km long circular accelerator, which provides collisions with a center of mass-energy of 7 TeV in p-p collisions and 2.76 TeV per nucleon in Pb-Pb collisions. This will be boosted up to 13 TeV in p-p and 5.5 TeV per nucleon in Pb-Pb in 2015. The LHC hosts a number of detectors, but we will be only using data from the ALICE-detector. This detector was built with the purpose of studying Quark Gluon Plasma (QGP).

1.1 Quark Gluon Plasma

The QGP is a state of matter which occurs at very high density and temperature. The building stones of hadronic matter, quarks, are confined as predicted by Quantum Chromodynamics, the theory on this subject. This means that it is impossible to seperate quarks from one another, and can only be found in their hadronic states. The same theory however, predicts that at very high temperature and/or density quarks can become free particles. This state is called the QGP. The QGP has a short lifetime (10fm/c) and we cannot observe it directly. So we want to look at the particles that travel through the hot and dense QCD matter and try to deduce the QGP properties from there. In proton-proton collisions, the system is too small to create a detectable QGP. But the Pb-Pb collisions provide an energy and density for an observable QGP. p-p collision study is still required to understand what happens in Pb-Pb collisions though. One of the methods to study the QGP is to look at the yield of hard scattered particles. As particles travel through a QGP they interact with the medium and lose momentum or potentially get completely absorbed. So by counting the yield of hard scattered particles we can get information about the QGP. Of course we need to compare these values to collisions without a QGP present and that is where the p-p collisions come in. p-p collisions provide a baseline for these studies. As there is no QGP produced in p-p collisions, they represent the vacuum reference value for particle yields. We then have to scale to compare the two. For this we use the nuclear modifcation factor: R_{AA} which is the ratio between the yield in heavy ion collisions and the yield in proton-proton collisions, normalised

using binary scaling. Formally:

$$R_{AA}(p_T) = \frac{dN_{AA}/dp_T}{\langle T_{AA}\rangle d\sigma_{pp}/dp_T}$$

where dN_{AA}/dp_T is the normalised yield measured in heavy-ion collisions, $\langle T_{AA}\rangle$ is the average nuclear overlap function (defined as the convolution of the nuclear density profiles of the colliding ions in the Glauber model) in the considered centrality range, and $d\sigma_{pp}$ is the production cross-section in proton-proton collisions.

1.2 D^* and B^0 mesons

In this Thesis we will study the D^{*+} and B^0 meson and their decay modes. The B^0 meson constists of a beauty anti-quark and a down quark, the D^{*+} meson consists of a charm quark and a down anti-quark. The reason to pick these particles to study the QGP is because the charm and beauty quarks have a relatively high mass and are therefore created early in the collision process, thus having time to travel through the QGP and not be created when the QGP is not even present anymore. Besides that, higher mass quarks are expected to lose less mass than light quarks and gluons. Our main channel we will be looking at is:

$$B^0 \rightarrow D^{*+}\pi^-$$
$$D^{*+} \rightarrow D^0 + \pi^+$$
$$D^0 \rightarrow K^-\pi^+$$
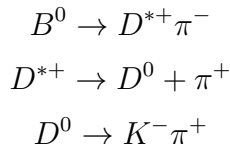
. The B^0 decay mode has a branching ratio of $2.76 \pm 0.13 * 10^{-3}\%$[1], the D^{*+} decay mode has a branching ratio of $67.7 \pm 0.5\%$ and the D^0 decay mode has a ratio of $3.89 \pm 0.05\%$. Because of this we need a lot of B^0 mesons to produce proper statistics on the D^{*+} and D^0 mesons. For this reason we also include a secondary channel, in our study:

$$B^0 \rightarrow D^{*+}\ell^+\nu_\ell$$

Where the lepton is usually an electron and so the neutrino an electron neutrino. The plus of this decay mode is that the branching ratio is $5.01 \pm 0.12\%$. The downside is that detecting the neutrino is impossible with ALICE detector. This gives us a larger deviation in the D^{*+} momentum.

This Thesis consists of two parts:

1. Computing the systematic error on yield extraction of the D^{*+}-meson from Pb-Pb collisions at ALICE and the efficiency of the Particle Identification

(PID).

2. Comparing the B^0 production in the current ALICE setting and after the accelerator has been upgraded, using the event generator PYTHIA. And study the properties of the B^0.
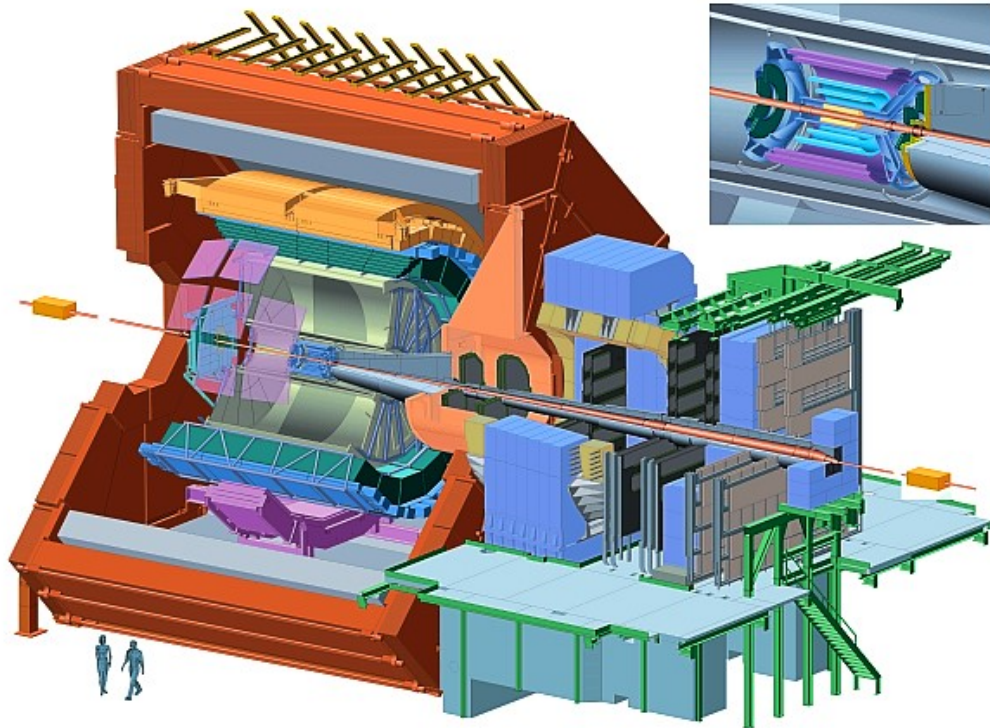
2   The ALICE detector

Figure 1: Scetch of the ALICE detector

ALICE, A Large Ion Collider Experiment, is a 26 m long, 16 m wide and 16 m high detector. To start of we would like to know the limitations we experience from the construction of the detector. The main variable in this discussion is η, the pseudorapidity. η measures the angle in respect to the direction of the particle beam. 0 being perpendicular and infinite being parrallel to the beam axis. The central barrel has an acceptance range of $|\eta| \leq 0.9$. And it consists of (from inside to outside) the Inner Tracking System (ITS), the Time Projection Chamber (TPC), the Transition Radiation Detector (TRD, which is used for electron identification), the Time Of Flight (TOF), the

High Momentum Particle Identification Detector (HMPID, which is used to determine the energy of very high energetic particles) the Photon Spectrometer (PHOS , which is used to study the inital phase in have ion collisions and jet-quenching) and the Electromagnetic Calorimeter (EMCal);. For this study we are not interested in electrons, very high energetic particles or jets. Therefore in the following only the ITS, TPC and TOF are discussed in depth.
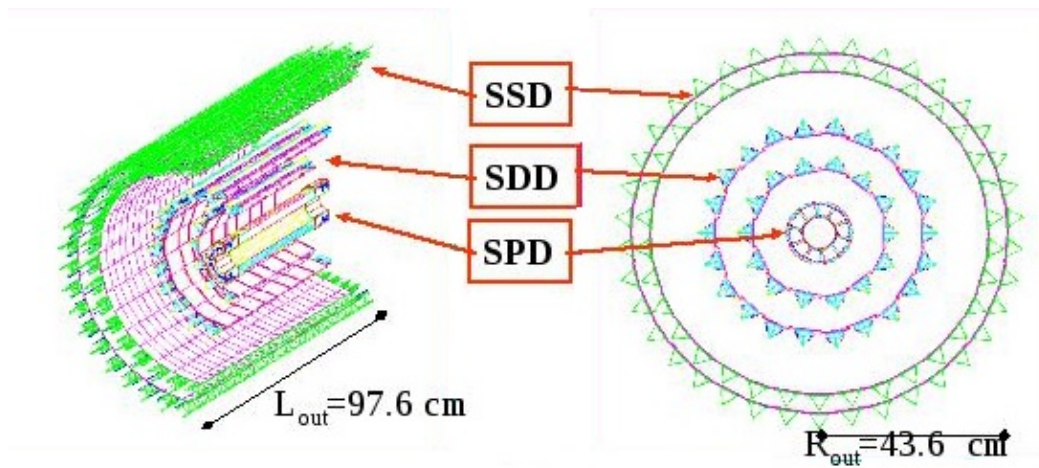
2.1 The Inner Tracking System

Figure 2: Scetch of the Inner Tracking System.

The ITS consists of 6 cylindrical layers of silicon, where the closest one to the beam pipe has a radius of 3.9 cm and the farthest away one has a radius of 43.0 cm. The six layers can be divided into three pairs: two Silicon Pixel Detectors, two Silicon Drift Detectors and two Silicon Strip Detectors (from inside to outside). The difference is in the resolution these detectors provide. The closer to the beam, the higher the particle density. In $\rho\phi$ (around the circle) the Pixel detectors provide a precision of 12 μm, the Drift detector a precision of 38 μm and the stripdetector a precision of 20 μm. In the z-direction (along the beamaxis) the precision is 100 μm, 28 μm and 83 μm. The primary use of the ITS is to identify the primary and secondary vertexes. The outer two layers also connect the tracks to those of the TPC and they do energy deposition measurements, which improves the momentum resolution.

6
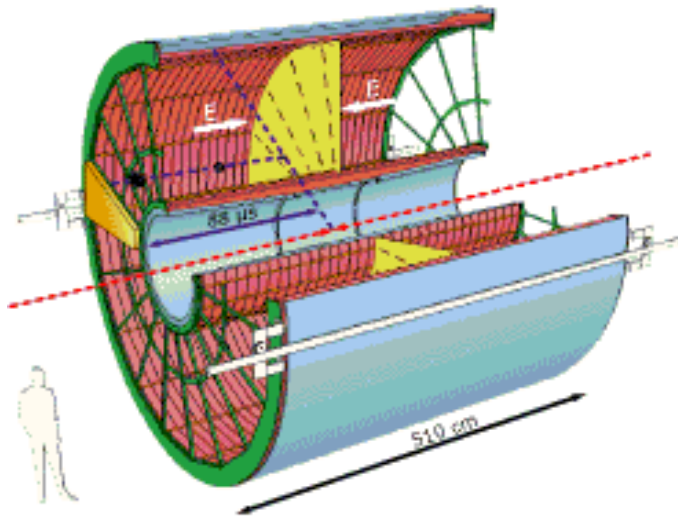
2.2 The Time Projection Chamber

Figure 3: Scetch of the Time Projection Chamber.

The TPC is a 5.1 meter long cylindrical gas chamber, with a volume of 88m^3. Charged particles ionize the gas, leaving behind a trail of ionized gas. To get a high momentum resolution and the capability to handle a lot of particles, a gas was needed with low diffusion, low compressibility and large ion mobility. Originally this led to a gas composed of 90% Neon and 10% CO_2, allthough later 5% Nytrogen was added. The traces move towards the end plates with a constant velocity, where wire planes and 560.000 electronic channels wait to detect the properties of the trace (the shape of the trace and the density of the ionisation). This way the TPC can give up to 159 space points with a position resolution of 1100-1250 μm in the rϕ plane and 800-1100 μm in the z-direction. From these traces we can deduce several values. Depending on the electrical charge and momentum of the particle, the trace will bend stronger or weaker. And the density of the ionisation depends on the momentum and identity of the particle. This contributes to the Particle Identification (PID) due to the specific ionisation energy loss (dE/dx)(see figure 4).
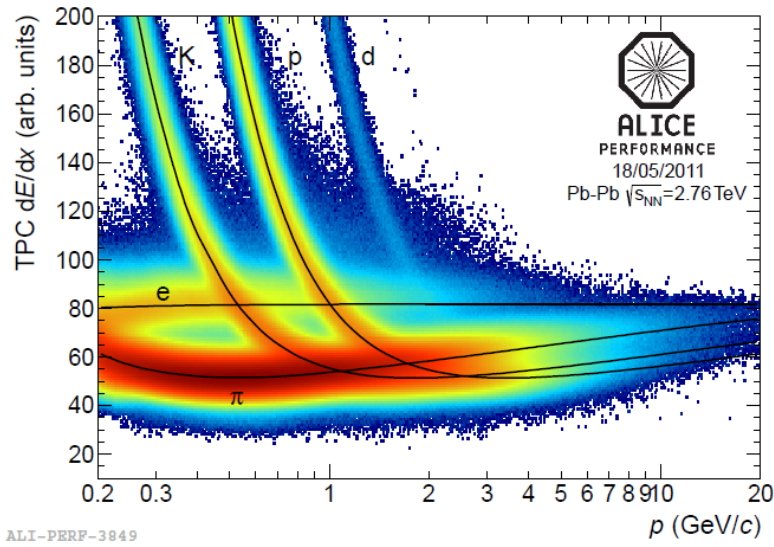
Figure 4: Specific ionisation energy loss for charged particles in the TPC as a function of the particle momentum. This graph shows the energy loss for 5 different particles in Pb-Pb collisions at 2.76 TeV per nucleon.
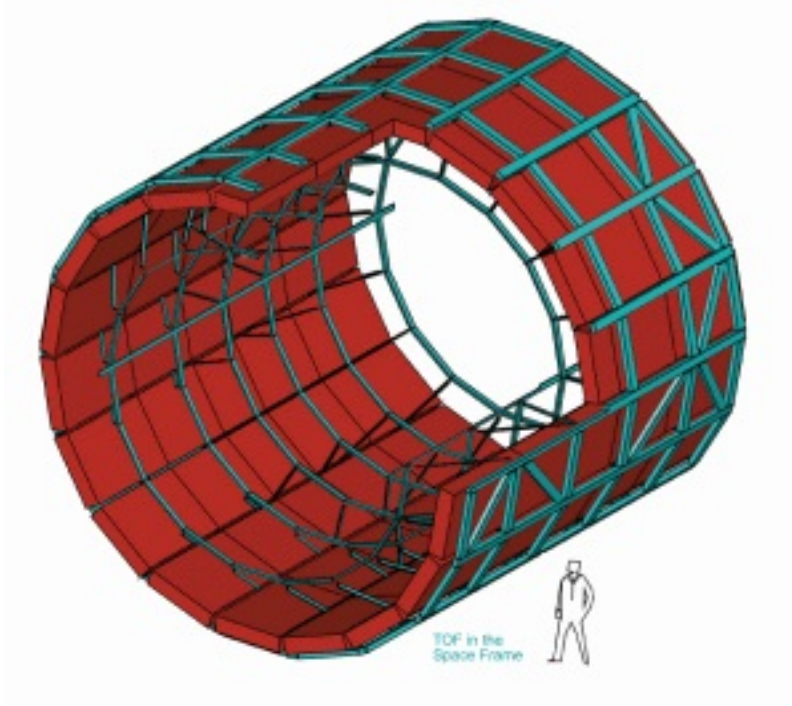
2.3 The Time of Flight

Figure 5: Scetch The Time of Flight.

The TOF has a cylindrical shape. It is divided into 90 pads, 18 in ϕ and 5 in the z direction. These pads contain a total of 1638 detectors (MRPC strips), which combined provide a total of 157248 readout channels. These Multigap Resistive Plates Chambers (MRPC) are stacks of resisitive glass plates (figure 6).
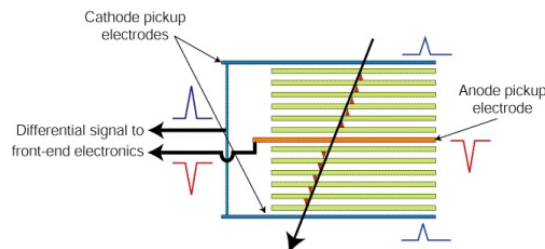

Figure 6: A single unit of Multigap Resistive Plates Chambers.

A high voltage is applied to the surface of the stack. And further out there are pickup electrodes. A charged particle ionises the gas and the high

electric field snowballs this effect into an electron avalanche. The glass plates stop this avalanche but are transparent to the signal induced on the pickup electrodes. So the total signal is the sum of the signal from all the gaps. More pads means higher accuracy, but more pads also means more downtime. The MRPC now has a time resolution of around 100ps. The time measurement with the TOF, coupled with the momentum and track length measured by the tracking detectors is used to calculate the particle mass. A time resolution of 100 ps will provide 3σ π/K separation up to 2.2 GeV/c and K/p separation up to 4 GeV/c. The information on flight times is used for PID (see figure 7).
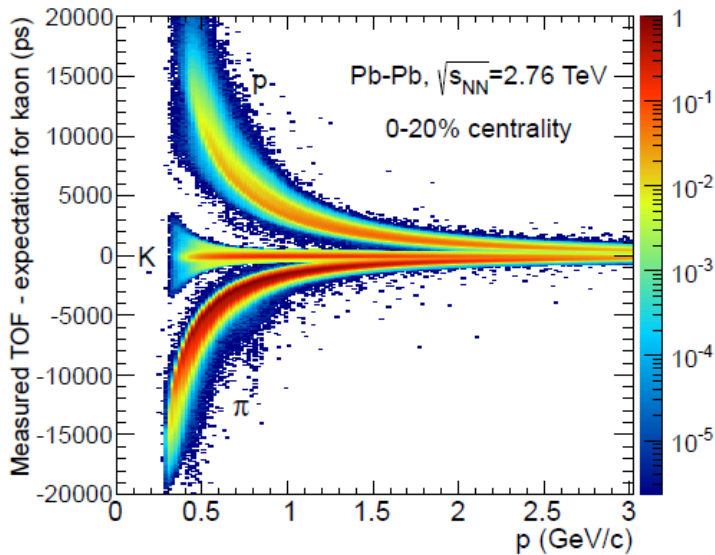

Figure 7: Difference between the measured time-of-flight and the expected value assuming the measured particle is a kaon as a function of the track momentum. These results are from Pb-Pb collisions.

3 D^{*+} analysis

As mentioned before, we are intrested in the decay mode: $D^{*+} \to D^0\pi^+$, from which the D^0 decays to $D^0 \to K^+\pi^-$. To reconstruct the D^{*+} we must reconstruct the D^0 first. But we are not able to observe the D^0 directly, as it decays after 120 μm. What we do observe are its daughter particles K and π. The D^0 decays into one negative and one positive, which are combined to form a list of candidates for the D^0. For these candidates, the invariant mass is calculated:

$$M(K\pi) = \sqrt{(E_K + E_\pi)^2 + (p_K + p_\pi)^2}$$

Here p is the momentum of the K and π particle and E is the energy of the particle. E is defined by: $E^2 = p^2 + m^2$. Where m is the value for the restmass provided by the Particle Data Group (PDG). By doing this we combine the tracks from the D^0 decay, but we also produce a lot of background. This background exists of all the uncorrelated pairs.

To find the D^{*+}, we combine the D^0 candidates to the remaining positive tracks (the π^+ from the $D^{*+} \to D^0\pi^+$ decay mode). We then add this π^+ in our invariant mass equation to give:

$$\Delta M = M(K\pi\pi) - M(K\pi)$$

We would like to do the same for the B^0, but due to the low statistics there was no signal to be found in ALICE data. Therefore the rest of this chapter and the chapter on real data is only about the D^{*+}.

3.1   Track quality cuts

To decrease the background and try to increase the quality on our tracks, there are some cuts applied on the single tracks:
- ITS refit;
- TPC refit.
This means that when a track is fitted from the ITS to the TPC, it gives the same track as when we fit it from the TPC to the ITs. We require:
- A minimum of one hit in the SPD
- A minimum p_T of 300 MeV/c
We also require the π^+ from the D^* to have a minimum p_T of 60 MeV/c.

3.2 Track topology cuts

For further decrease of the background, there is a selection on the topology of the tracks. The D^{*+} decays through a strong process, so the decay length is very short. It is in fact lower than the detector resolution, meaning we can't distinguish the point at which the D^{*+} decays and where the D^0 decays. So the D^0 is at the primary vertex.
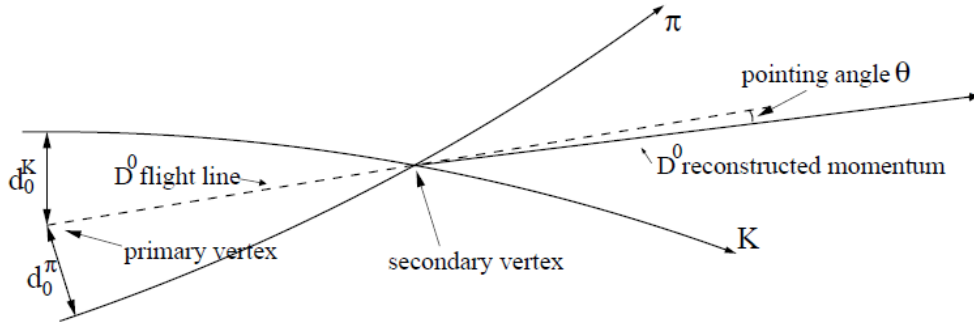

Figure 8: Topology and relevant variables of a D^0 meson decay, for which a primary and secondary vertex have been reconstructed.

Next, we extrapolate the kaon and pion tracks. We then define the impact paramater as the closest approach between the track and the primary vertex. This gives us the impact parameters $d^K{}_0$ and $d^\pi{}_0$. From this we also get the distance of closest approach (dca). We can compute the angle between the line that is drawn from the primary vertex to the secondary vertex and the line that represents the reconstructed D^0 momentum, which we name: θ_{point}. We can then place cuts on all these variables, as well as the prodcuct of the impact parameters and the momenta of the kaon and the pion. We also cut on the cosine of the angle between the flight line and the kaon momentum in the D^0 rest frame: θ^*. Aside from these selection criteria, there is the Partice Identification (PID) cut. A $n\sigma$ PID cut means that only particles that have been identified with at least a probability of $n\sigma$ are selected. The standard value for n is 3.

3.3 Invariant mass analysis

As mentioned before, when we look at the D^*, we compute the difference in invariant mass between the D^{*+} and the D^0:

$$\Delta M = M(K\pi\pi) - M(K\pi)$$

This gives us a distribution that starts at the mass of the pion and peaks at the mass difference between the D^{*+} and the D^0.
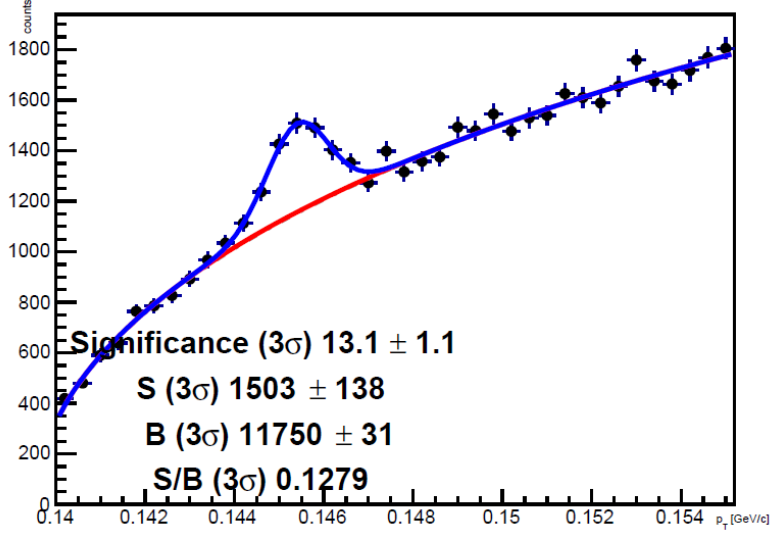

Figure 9: The invariant mass distribution for the D^{*+} integrated over p_T.

Due to the nature of the selection (combining everything and then trying to select), we get a clear combinatorial background. The peak, and everything under it, represent the real D^{*+}. We call this area under the peak: the raw yield. To fit the histogram we define two functions: f_{gaus} and $f_{background}$. First we fit the region outside of the peak (3σ) with the background function:

$$f_{background}(x) = a(\Delta M - m_\pi)^{1/2} e^{b(x-m_\pi)}$$

Where a and b are fit constants and m_π is the mass of the pion. Then we fit the entire histogram, keeping a and b fixed, with the f_{gaus} added to the background function:

$$f_{gaus}(x) = \frac{c}{\sqrt{2\pi d^2}} e^{-\frac{(x-e)^2}{2d^2}}$$

Where c, d and e are fit parameters, d being the width and c being the yield.
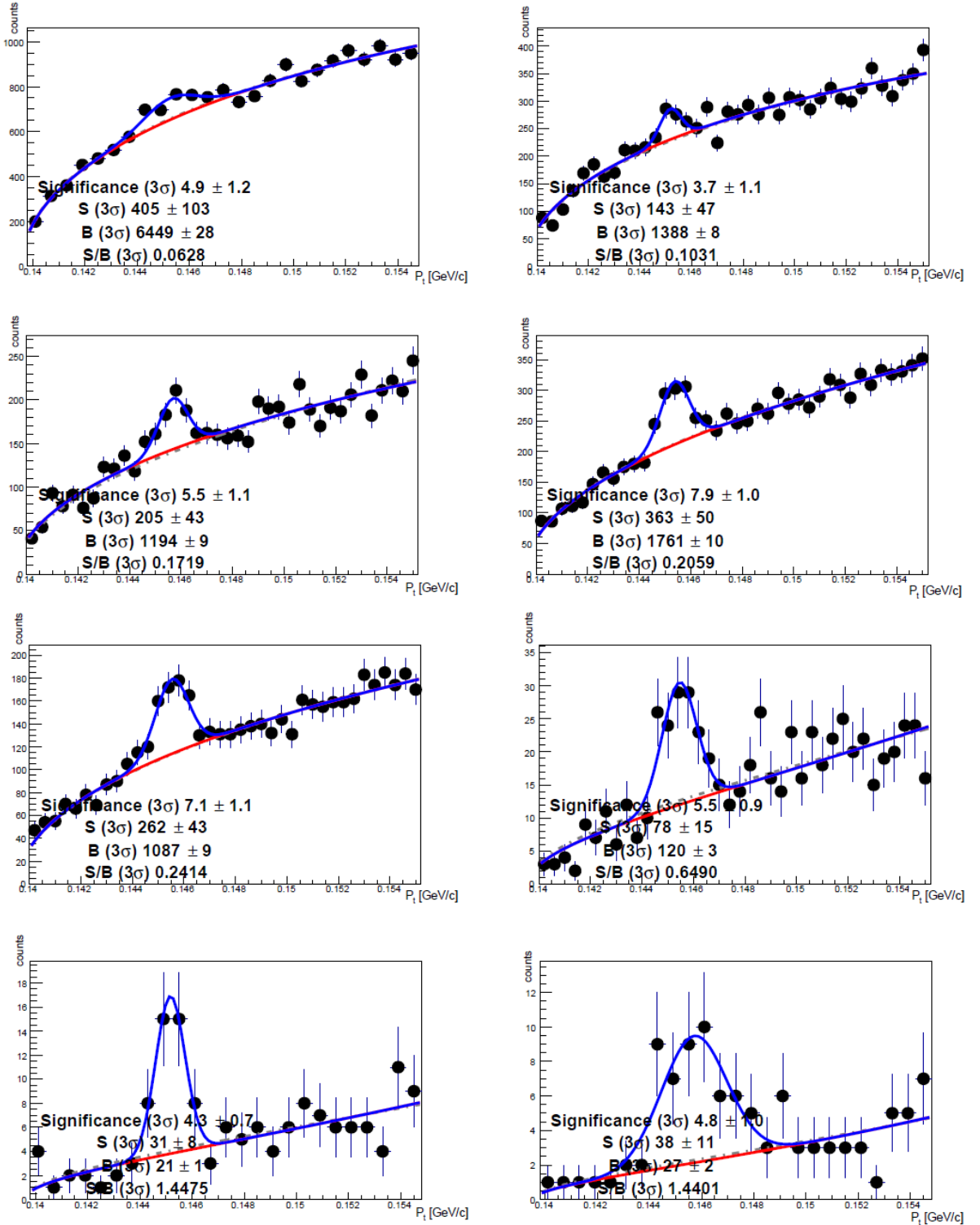
13

14

Figure 10: The p_T distribution for the D^{*+} in p_T bins (3-4, 4-5, 5-6, 6-8, 8-12, 12-16, 16-24, 24-36). The points are the bin contents, in blue the total fit ($f_{gaus} + f_{background}$) and in red only the fit on the background.
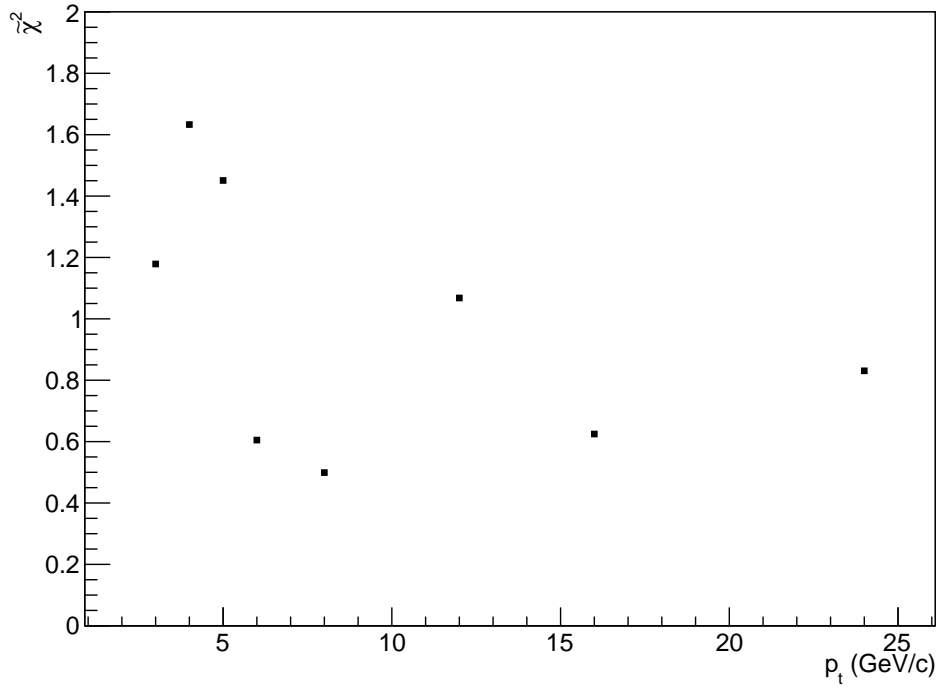
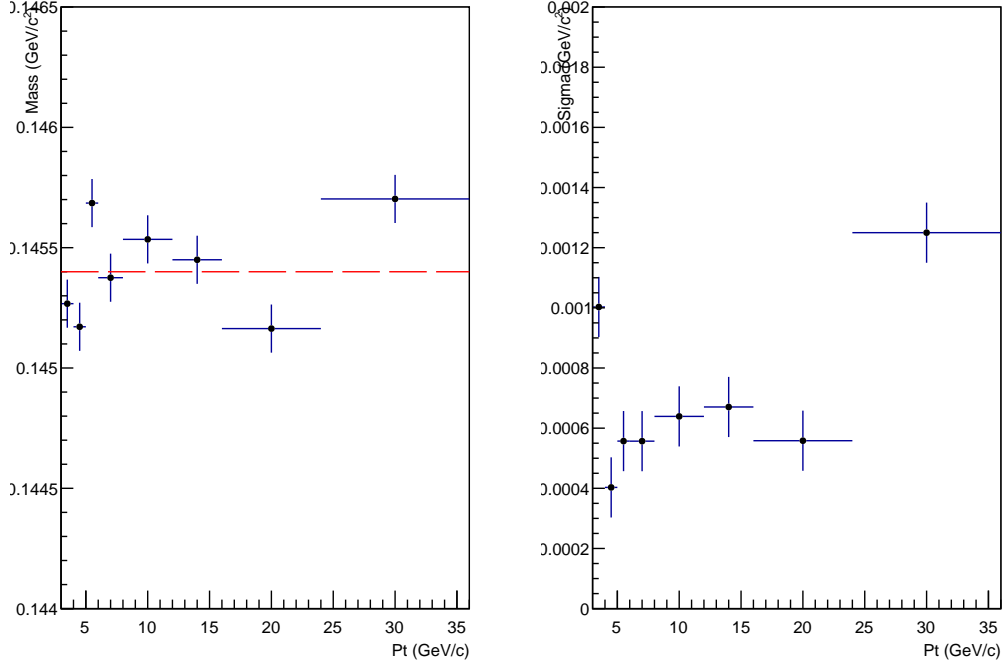Figure 11: $\tilde{\chi}^2$ for the fits in all the different bins.

15

Figure 12: The position and width of the gaussian fit as defined in the previous section. The dashed red line is where the peak should be.

4 Yield extraction

This chapter will focus on the systematics on the yield for the different p_T bins and the error that we estimate by extracting the yield in multiple ways. As mentioned, the raw yield is the area under the gaussian. Here in a table along with the signal divided by the background (S/B).

p_T range (Gev/c)	Signal	S/B
3-4	405	0.0590
4-5	143	0.0898
5-6	205	0.1719
6-8	363	0.2059
8-12	262	0.2414
12-16	78	0.6490
16-24	31	1.4475
24-36	38	1.4175

16

4.1 Methods

We will extract the yield in different ways, which gives us a systematic uncertainty. We compare the value to value we get from bin counting, which simply counts the entries in the bins in a 3σ range around the centre of the peak and substracts this by the background function. The division from the yield from bin counting by the raw yield is the yield ratio.

4.1.1 Background function

Instead of using the before metioned function for the background, we can use an alternative function:

$$f_{background2} = a(x - m_\pi)^b$$

4.1.2 Fit range

The standard interval to fit is done by fitting from 0.135 to 0.155 GeV/c^2. We test the ranges 0.135 to 0.160 GeV/c^2 and 0.135 to 0.165 GeV/c^2.

4.1.3 Systematics

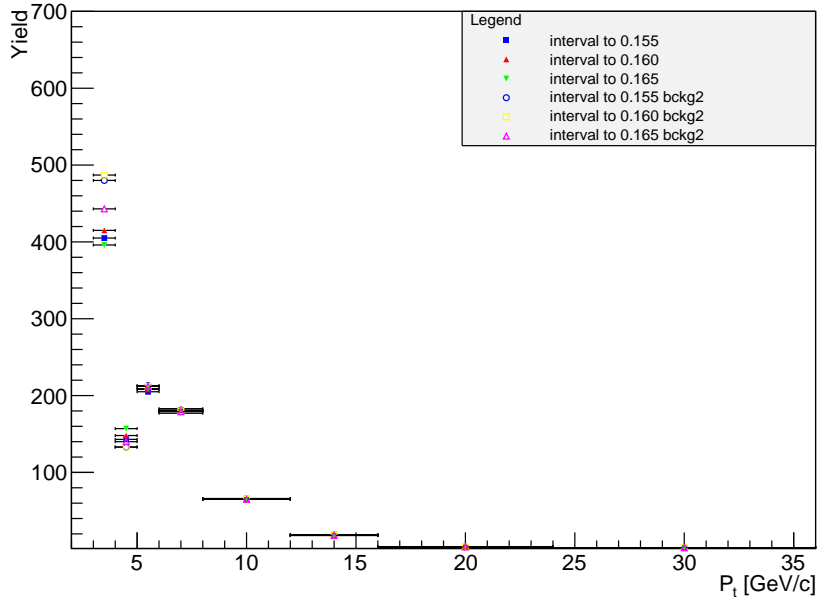All these different methods give us different yields and yield ratios.

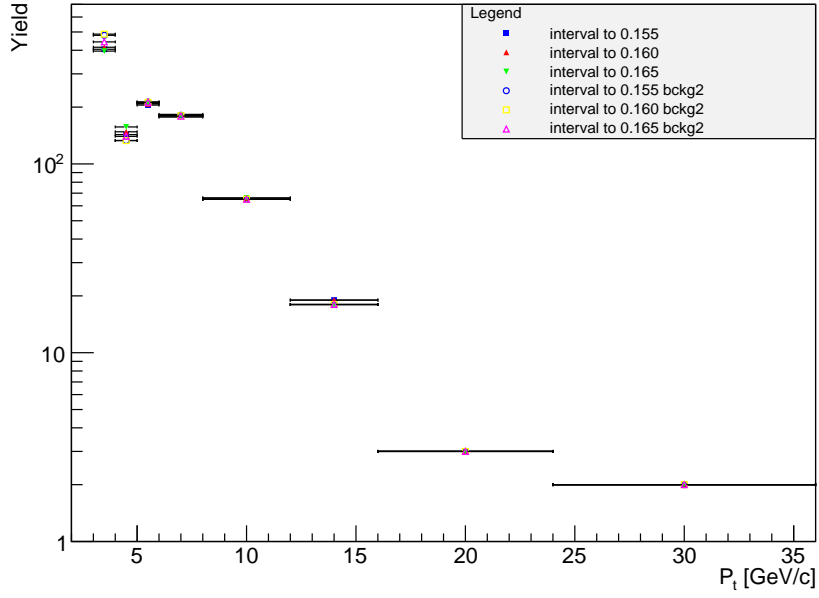Figure 13: The raw yield for different fitting ranges and background functions.

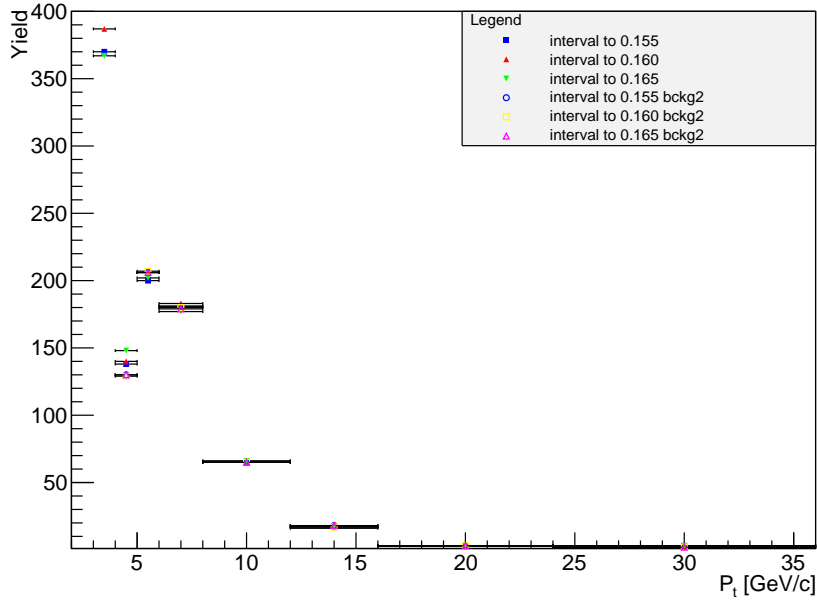Figure 14: The raw yield for different fitting ranges and background functions woth logarythmic scale.
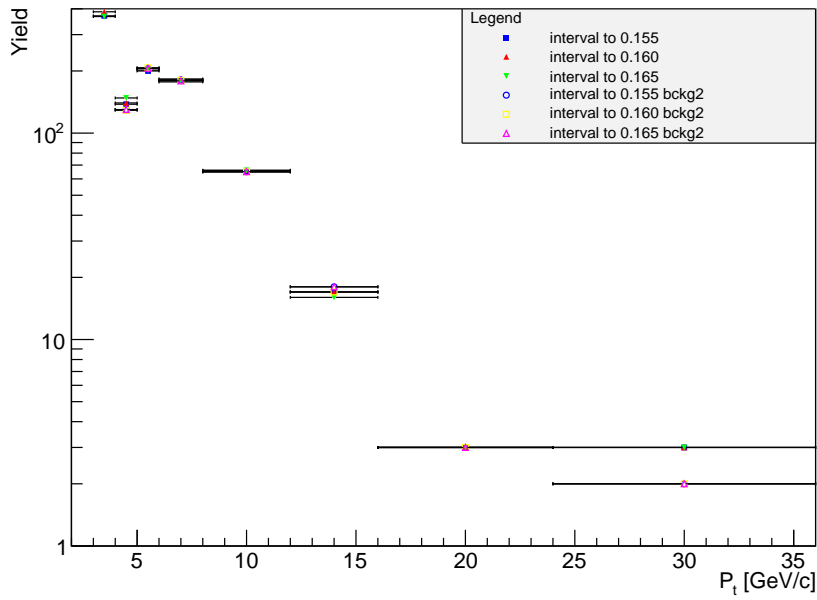
Figure 15: The raw yield from bin counting.

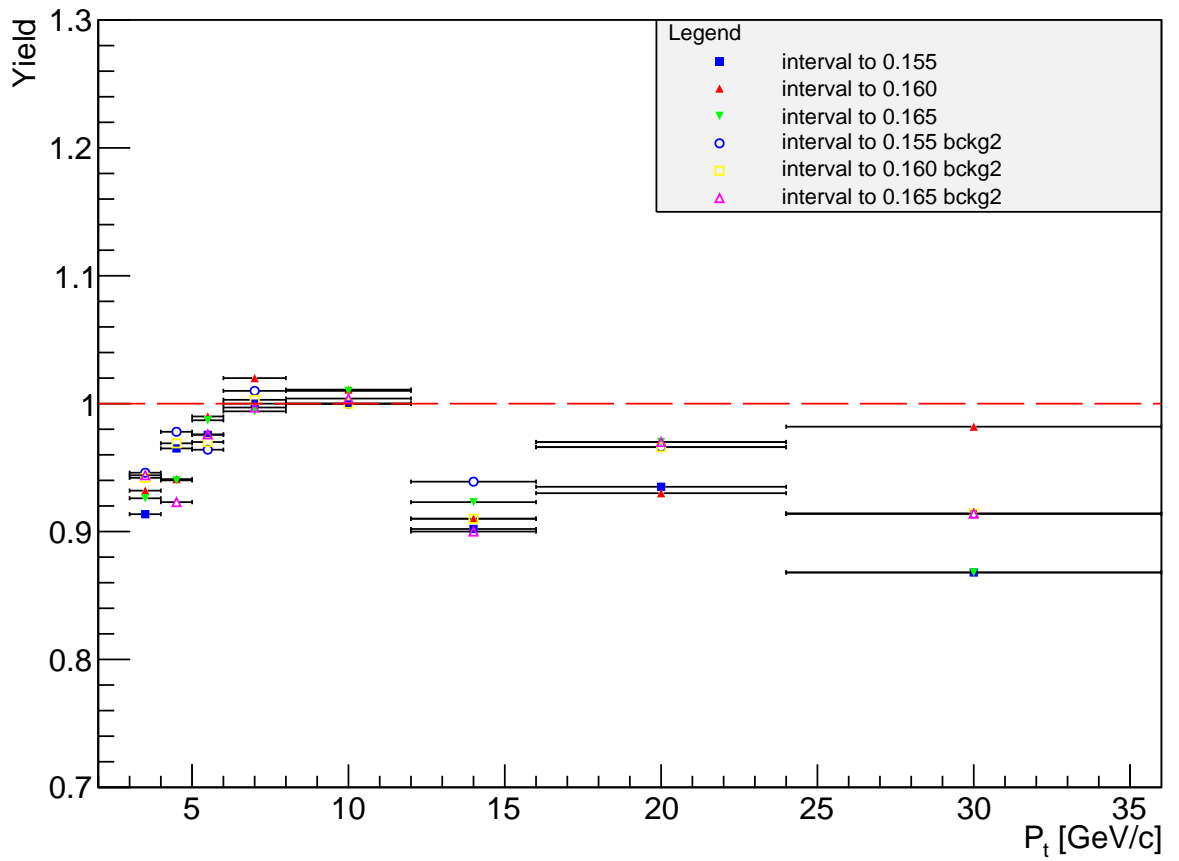Figure 16: The raw yield from bin counting with logarythmic scale.

20

Figure 17: The ratio of the yield from bin counting over the yield from the fit. The dashed red line represents the values we would get if there was no systematic uncertainty.

4.2 Particle Identification

The Particle Identification (PID) is based on the methods described in the sections about the TPC and TOF(2.2 and 2.3). For p-p and Pb-Pb cuts were made for the expected specific ionic energy loss (dE/dx) for the TPC and the expected flight time for the TOF. These distributions (see figure 4 and 7) can be described by a gaussian function. The selections were based on the width σ of these distributions, where ideally a 3 and 2 σ cut would be 99.7% and 95% efficient for the signal for the two particle identification procedures. In doing this it rejects background up to a factor 3 in low momentum regions. To see if there is a systematic uncertainty in the PID we compare the values for the yield with PID to those without PID.
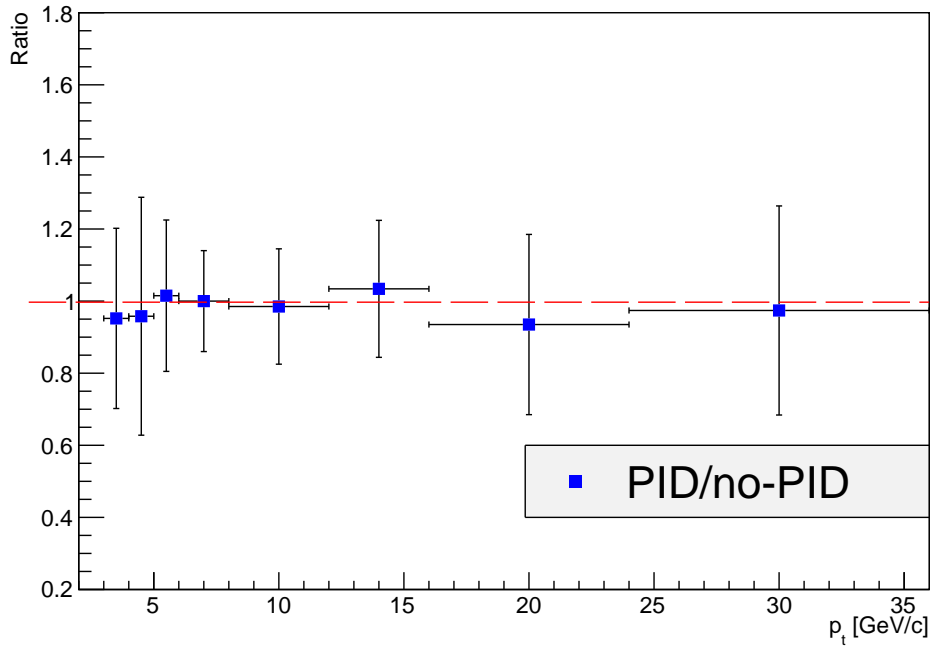

Figure 18: The ratio of the yield without PID over the yield with PID. The dashed red line represents the values we would get if there was no systematic uncertainty.

5 B^0 production study

As mentioned in the introduction we will also study the B^0 mesons. As mentioned before, we were unable to reconstruct a significant signal from the 2011 data from ALICE. However we would like to study this meson and its properties. For this we use the event generator PYTHIA. This program contains all the QCD laws and PDG values of branching ratios and particle energies. So basically it contains the model that we have created with theories about particle physics and quantitative information from research. This allows us to observe the physics without the limitations of a detector. All the particle data (type, energy, topology of tracks) is stored in the program and this makes event generators a very powerful tool to predict. We want to study the decay from B^0 and D^{*+} and aside from that we want to predict what we may see in 2015, when the LHC upgrades to a centre of mass energy of 13 TeV for p-p. Note that the procedure of calculating the B^0 is the same as for the D^{*+} (see chapter 3). We can add a pion and for the other decay we add an electron and an anti-electron neutrino.

5.1 Configuration

PYTHIA has the convenient option to choose which processes you can select. You can also scale them or force them. This, so you can optimize the events for the phenomenon you want to study. I will not bother you with all the code here, but I will show and explain the configuration chart:

-Beams: idA=**2212**
-Beams: idB=**2212**
This sets the two incoming beams to be protons.
-Beams: eCM=**13000**
This sets the center of mass energy to 13 TeV. For the 7 TeV collisions, this

value is of course set to 7000.

-HardQCD: all=on

This turns on all hard QCD processes.

-Partonlevel: MI=off

Turns off multiple interactions.

-Partonlevel: ISR=on

-Partonlevel: FSR=on

Turn on initial state radiaton (ISR) and final state radiation (FSR).

-SigmaProcess:alphaSorder=2

-SigmaProcess:renormScale=2

-SigmaProcess:renormMultfac=1

-BeamRemnants:primordialKT=on

-BeamRemnants: primordialKTsoft=0

-BeamRemnants:primordialKThard=1

BeamRemnants:halfscaleForKT=0

-BeamRemnants:halfmassforKT=0

These scale certain processes such as the decay of the α_s particle, the Q^2 normalisation scale for 1→2, 2→2 and 2→3 processes and primordial k$_T$ in multiparton interactions. These are standard values taken from the ALICE experiment.

-ParticleData:mcRun=**1.20**

-ParticleData:mbRun=**4.78**

Sets the mass for the beauty and charm quark to optimalize for our study. Again standard values taken from ALICE.

-HardQCD:gg2bbbar = on

-HardQCD:qqbar2bbbar = on

These last two are the most important ones in the configuration. With these we force the production of a $b\bar{b}$-pair through gluon splitting or scattering. PYTHIA randomly selects one of those two mechanisms, proportional to nature. Which is about 90% gluon splitting and 10% scattering. This greatly increases the amount of B^0 we get, as it consists of a beaty antiquark and a down quark. Now we have 1 $b\bar{b}$-pair per event, while normally we would have one per 50. The downside is that this is then no longer a minimum bias model. However, we think we can reasonably scale for this. And it greatly improves the statistics on the study. That is why we chose to force this process instead of using a minimum bias model. To futher illustrate this, recall the branching ratios from the introduction. We get about 3 D^* from $B^0 \rightarrow D^{*+}\pi^-$ per 1000 B^0. So we get about 3 D^0 that go into $D^0 \rightarrow K^-\pi^+\pi^0$ per 10000 B^0. To produce 10000 B^0 we require approximately 60 million events at 13 TeV. This take our normal computers almost 2 days. Not only

is this the reason to abandon a minimum bias model, it is also the reason to include another decay channel:

$$B^0 \to D^{*+}\ell^-\nu_\ell$$

Where we take the lepton to be an electron. The advantage of this channel, is that the branching ratio is $5.01 \pm 0.12\%$. This is 2000 times larger than our previous channel. As the neutrino is impossible to detect in the LHC, it is not as easy to create an invariant mass distribution in the same way as we did for the D^*. To calculate the momentum we take all the D^* and electrons and look for pairs. We then reconstruct the primary vertex from which they came. From this point we draw a line to the point of collision. That line is the B^0 flight line (the decay of the quark into the B^0 happens on a femtometer scale). Now if we calculate the momentum vector of the D^*-electron pair we see that it points in a different direction than the B^0 flight line. And from this we can calculate the missing momentum. The missing momentum is of course something different than the neutrino momentum, but it is in the same order. Therefore our invariant mass distribution would be more smeared out than the one we saw in the chapter on the D^*.

5.2 Data analysis

All the graphs are drawn from a data sample of 1.3 billion collisions, unless otherwsie mentioned. To illustrate the last remarks in the previous section, the next plot gives an overview of how much study material we get. The first bin is the total amount of B^0 that we get. The second bin contains the total amount of D^{*+} that decay from B^0. Bin 3,4 and 5 contain the 3 steps of our secondary decay channel starting with $B^0 \to D^{*+}e^-\nu_e$, where 4 and 5 are the same decays as our main channel. Bins 6, 7 and 8 contain our main channel.
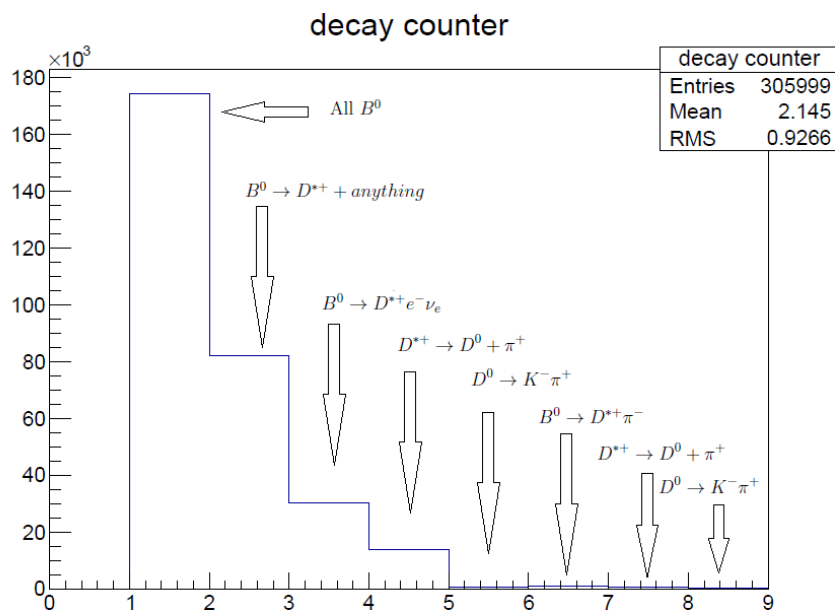
Figure 19: The amount of decays. In bin 1-2: all the B^0, in bin 2-3: all the D^* from B^0. Than the three steps of the decay: $B^0 \rightarrow D^{*+}el^-\nu_e$, $D^{*+} \rightarrow D^0\pi^+$, $D^0 \rightarrow K^+\pi^-$ in the bins 3-4, 4-5 and 5-6. And the three steps of the decay $B^0 \rightarrow D^{*+}\pi^-$, $D^{*+} \rightarrow D^0\pi^+$, $D^0 \rightarrow K^+\pi^-$ in the bins 6-7, 7-8, 8-9.
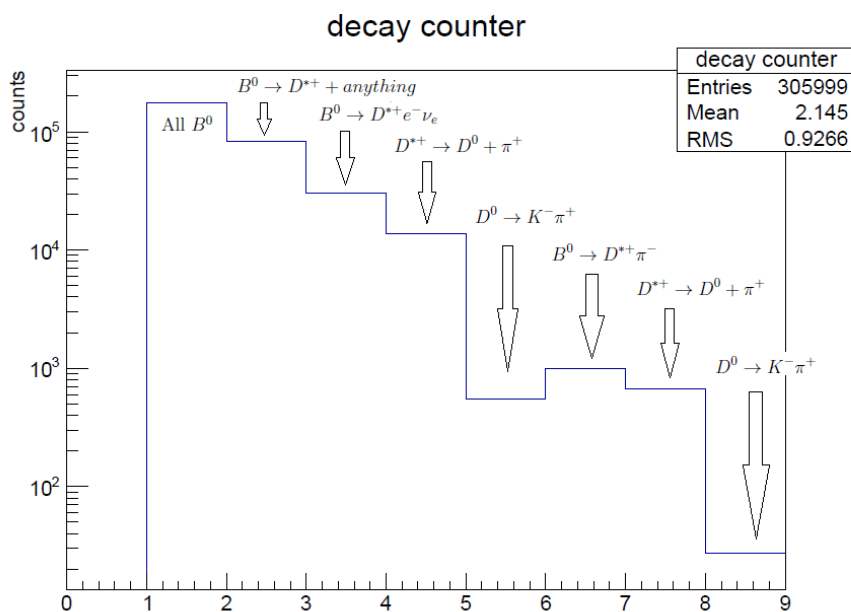

Figure 20: The same histogram as figure 17, but in logarythmic scale.

26

5.2.1 B^0 production study in 7 TeV and 13 TeV

To compare the 7 TeV collisions to the 13 TeV collisions we must look at a few things. We obviously expect there to be more B^0 production at 13 TeV, but we do not expect this to be a simple multiplication. First we look at the p_T distribution of the B^0, and at the same time compare the distribution we get for 13 TeV with that for 7 TeV. Now we can see not only what the increase in raw yield is, but also what kind of B^0 we gain the most in terms of transverse momentum.
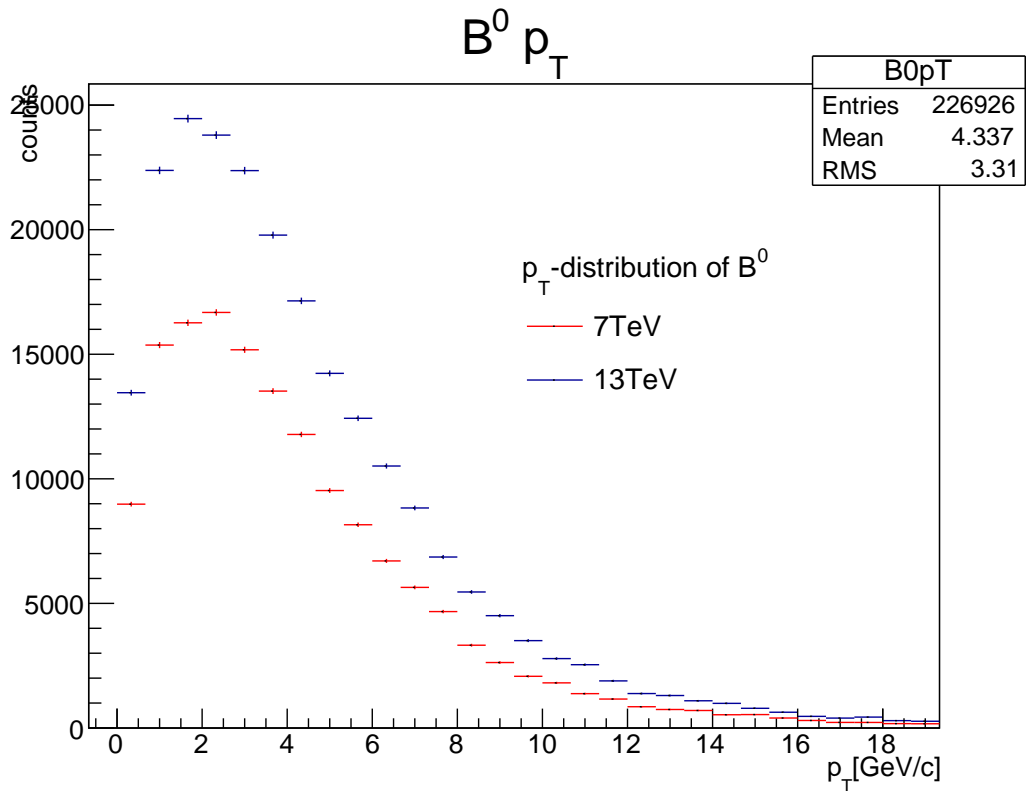

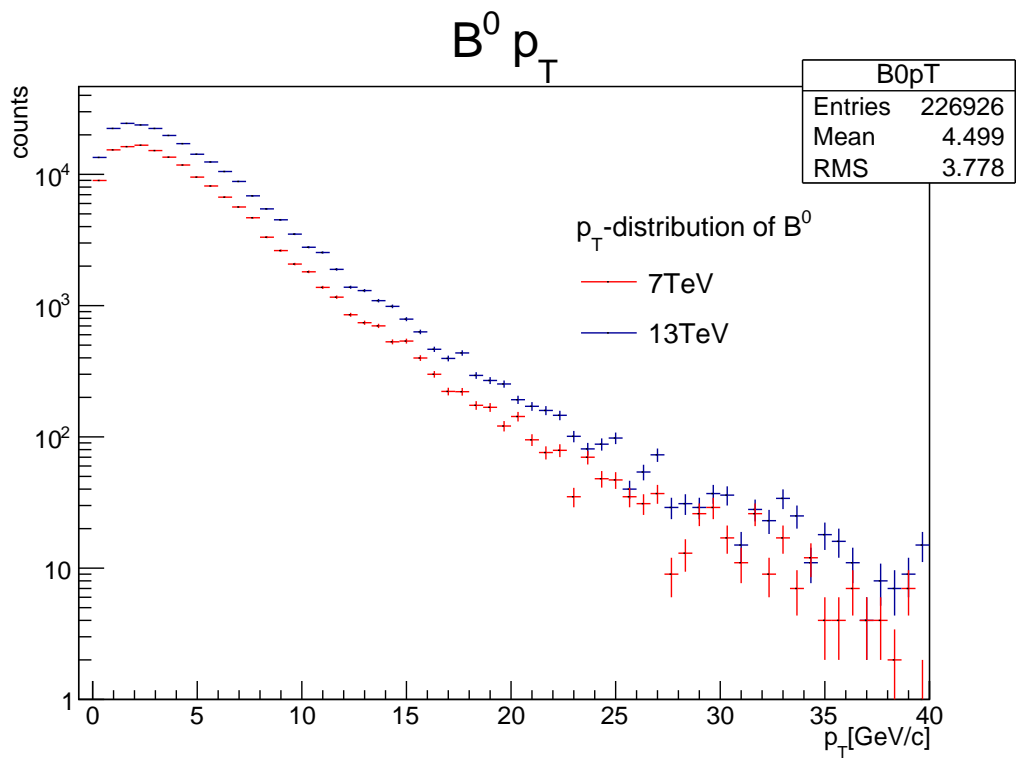Figure 21: The p_T-distribution of the B^0 at p-p collisions in PYTHIA at 7 TeV (red) and 13 TeV (blue).

27

Figure 22: The p_T-distribution of the B^0 at p-p collisions in PYTHIA at 7 TeV (red) and 13 TeV (blue) in logarythmic scale.
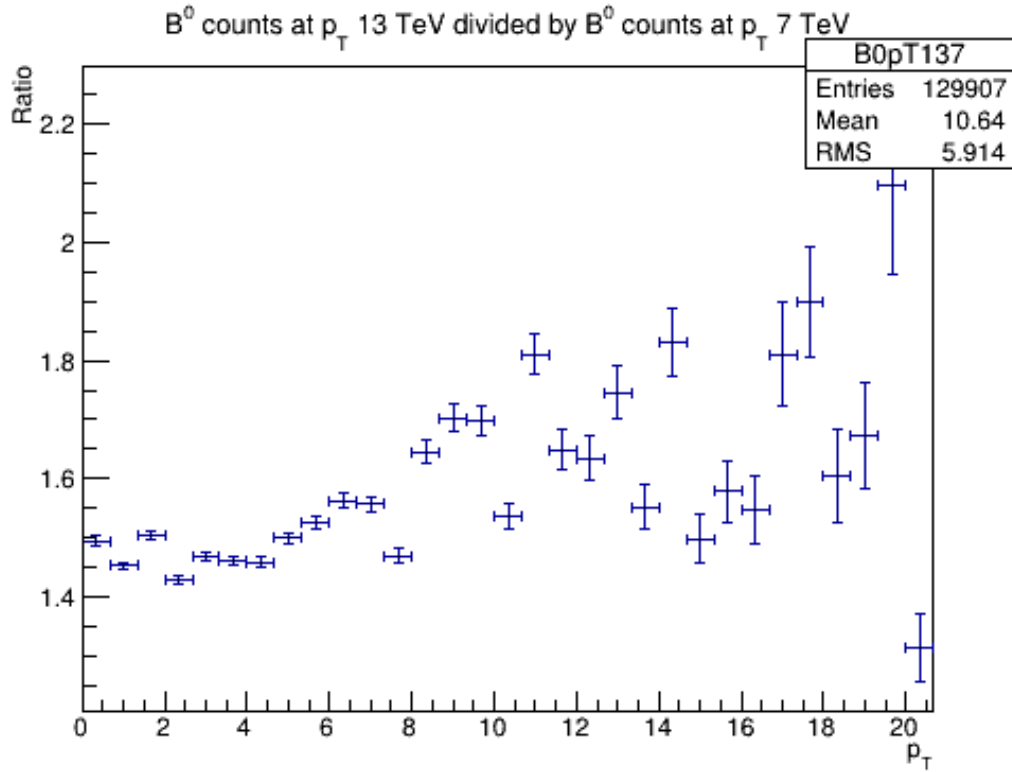
Figure 23: The ratio of the two distribution in figure 20.

We can see a rise of 51% in raw yield, and that the ratio is about 1.5 at low p_T and grows to 2 at high p_T. These are all the B^0 produced in the event generator. The ALICE detector obviously has some limitations. The first limitation we have to aknowledge, is on the pseudorapidity (see chapter 2). ALICE only detects for $-0.9 \leq \eta \leq 0.9$. So to see how much we miss we take a look at the η-distribution for the B^0:
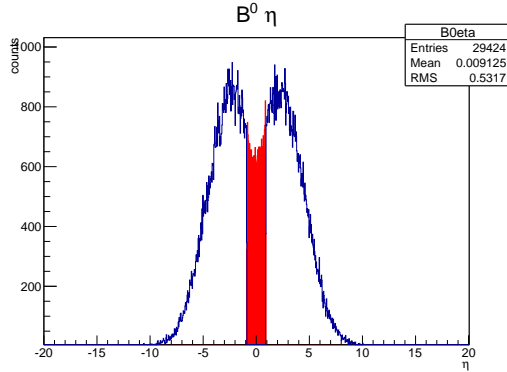
Figure 24: η-disribution for the B^0.
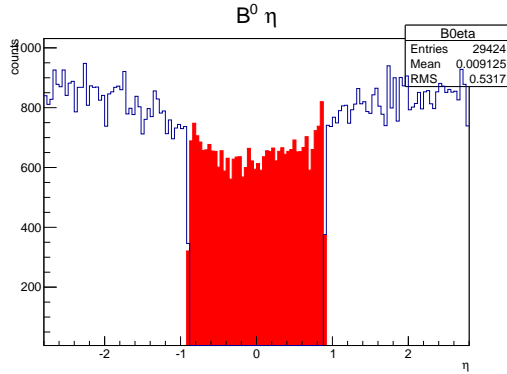

Figure 25: η-disribution for the B^0 zoomed in around the acceptance region: $-0.9 < \eta < 0.9$.

This cuts 85.7 % of our B^0 at 13 TeV. At 7 TeV we lose 85.4% To get more information about which B^0 we lose, we also look at the η-distribution in p_T bins. As we have seen, the ratio of 13 TeV/7 TeV B^0 production is not constant in p_T. Therefore it is interesting to see the η-distribution in p_T bins, because we can then see how the acceptance at the two different collision energies behaves.
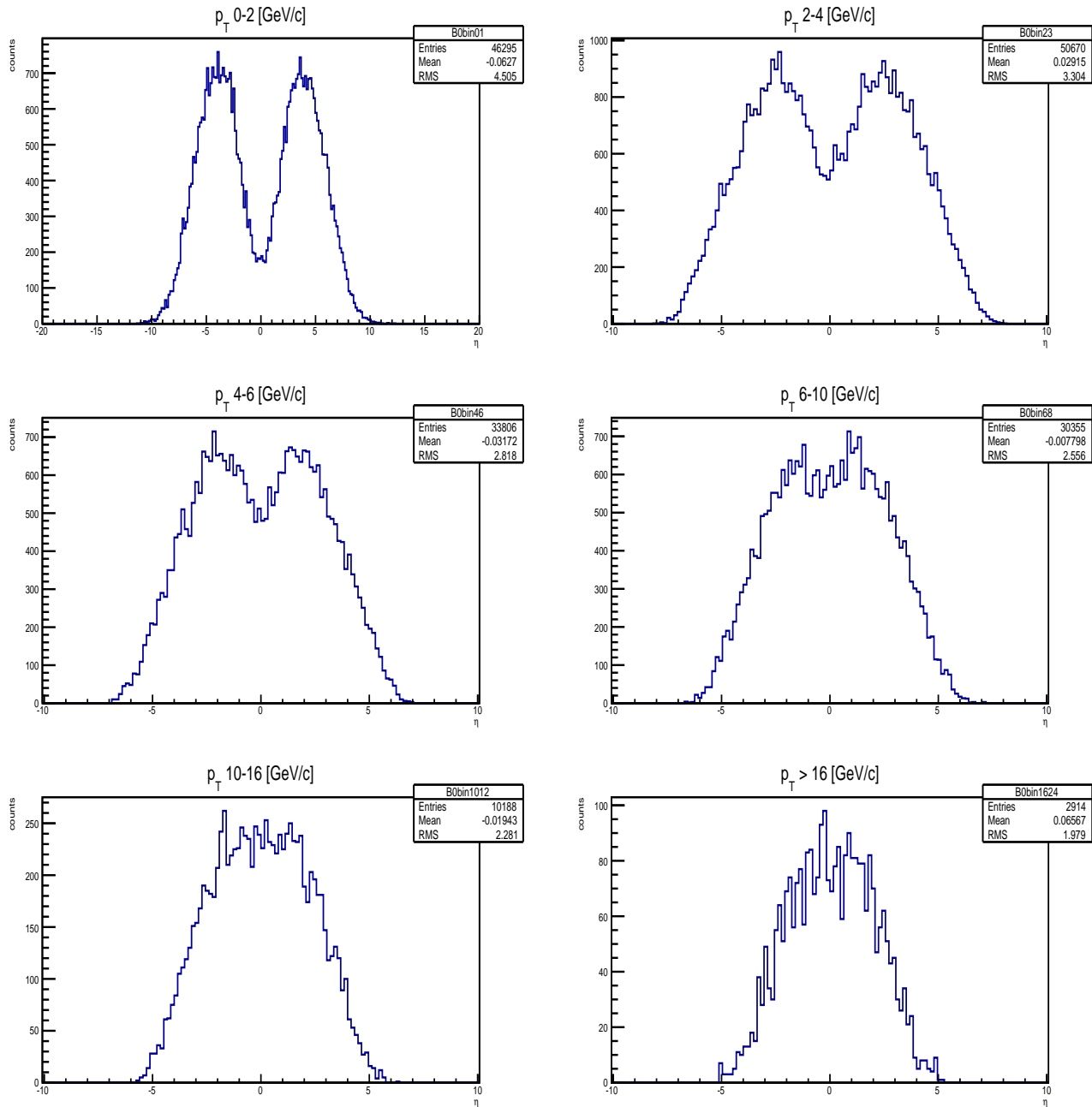
Figure 26: η-disribution for B^0 mesons in p_T bins at 13 TeV: 0-2, 2-4, 4-6, 6-10, 10-16 and <16 (in GeV/c).

From the previous figure we can conclude several things. The histograms

show us that the study of B^0 will be difficult at low p_T as most of the particles go outside of acceptance. Another question appeared as a result of these histograms. As we have seen in figure 20 the ratio of B^0 at 13 TeV over B^0 at 7 TeV rises slightly from low to high p_T. We have also seen that we have a slight loss in acceptance when we go from 7 TeV to 13 TeV. This does not compute with what we have found in figure 23. As the acceptance is higher at high p_T we would expect the 13 TeV sample to improve in acceptance as there are relatively more B^0 at high p_T compared to the 7 TeV data. For this reason we also include the same figure as figure 25 for 7 TeV.
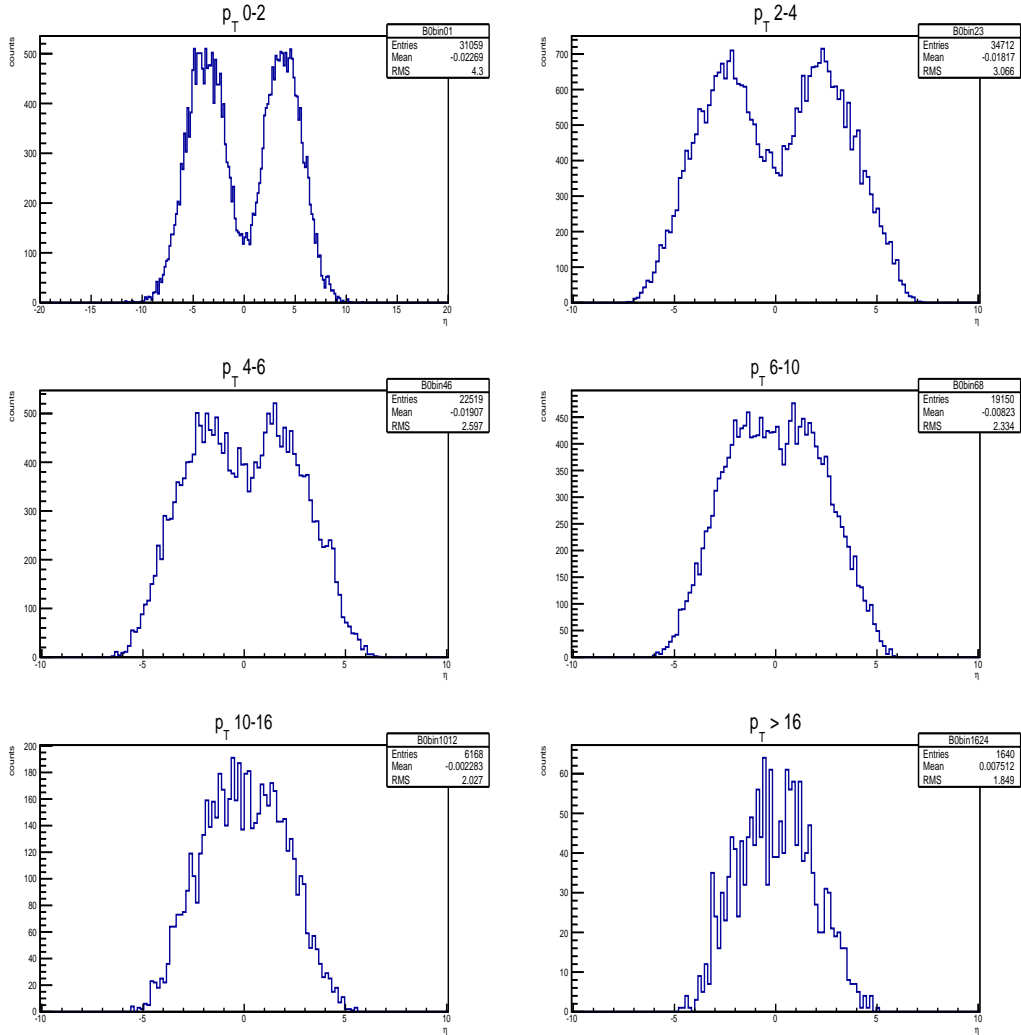
Figure 27: η-disribution for B^0 mesons in p_T bins at 7 TeV: 0-2, 2-4, 4-6, 6-10, 10-16 and ¿16 (in GeV/c).

Here we find the logical solution to the questionmarks posed after figure 26. We see that the standard deviation (RMS) is larger at 13 TeV than at 7 TeV. The distribution is more spread out, which would compensate for the effects we saw in figure 25. To further visualise this fact we have plotted the ratio of figure 25 and 26.
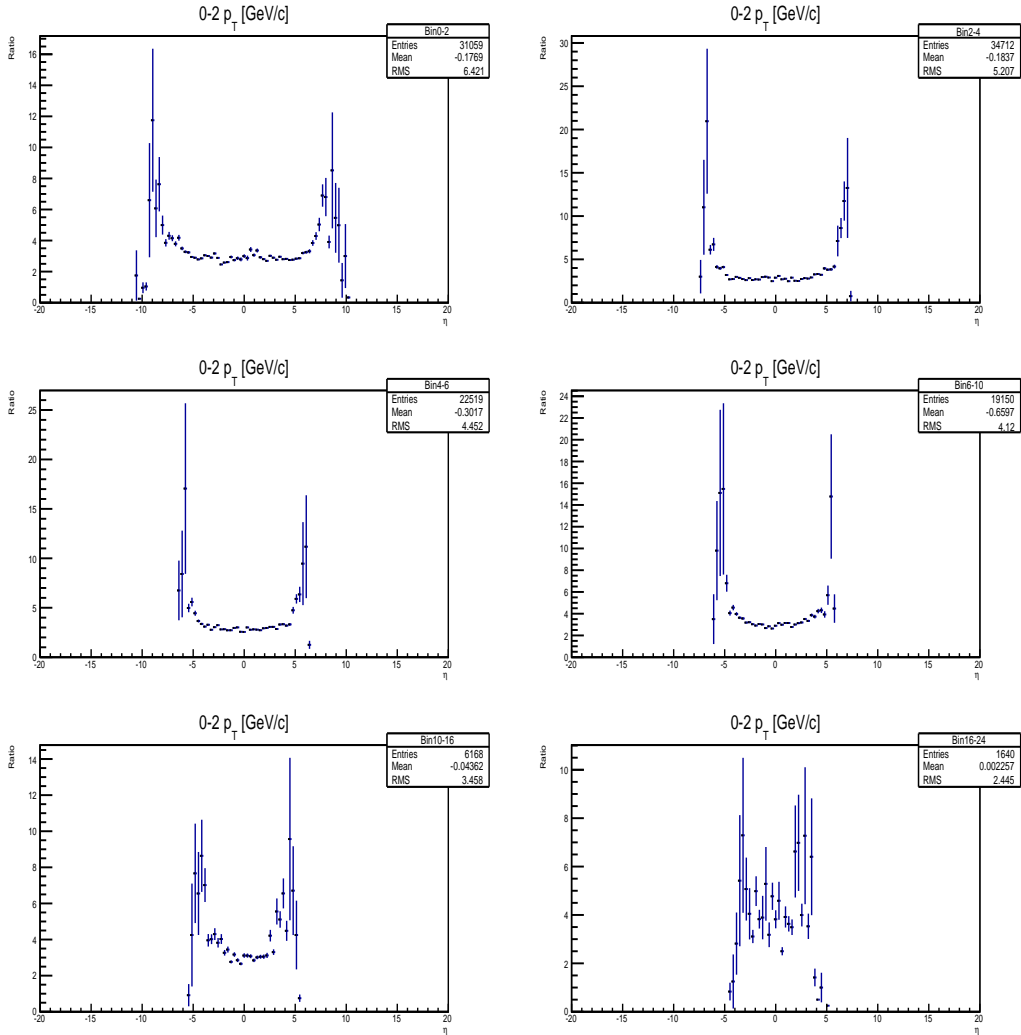
Figure 28: The ratio of figure 23 and figure 24.

Note that the 13 TeV dominates more towards the sides, further emphasising the beforementioned conlclusion.

What also appeared interesting was to see the relation in η between the B^0 and the beauty quark. As the beauty quark decays on a femtometer scale, we expect to see little difference between the two η distributions. But as we are forcing $b\bar{b}$-pair production, it was easy to check. The distributions for the beauty quark comes from a sample of 200 million events.
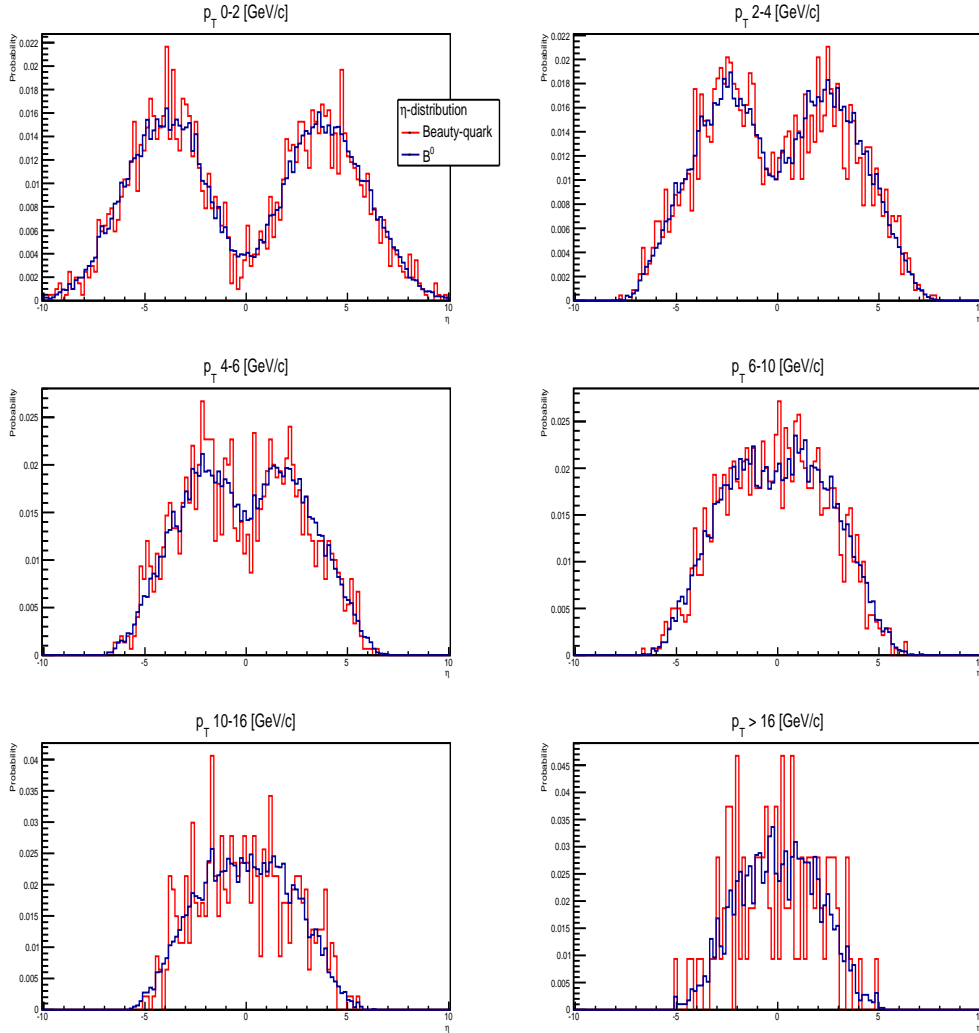
Figure 29: η distribution for the B^0 (blue) and the beauty- quark (red.)

As we can see the two distributions in figure 29 are approximately the same. To make the data comparable with what we expect in ALICE we have to take account for the other detector limitations, the amount of collisions we are going to get and the fact that we are not using a minimum bias model. In ALICE we will get 170 billions collisions. The $b\bar{b}$-pair production happens in nature approximately once every 25 collisions. For these two we can scale easily, and it comes out to ∼16 detectable B^0. The ALICE efficiency is harder to apply, as it is not constant over p_T.

5.2.2 Main channel D^* production

For the D^{*+} we are less interested in the 7 TeV to 13 TeV comparison. We can deduce our increased statistics from the B^0 as the branching ratio for our decay does not change. This means that we can focus on the properties of the particles and the relations they have in the specific decay. One of these things is comparing the properties of the 'regular' D^{*+} to the ones that come from our prefered decay(s). We will start by comparing the p_T distributions.
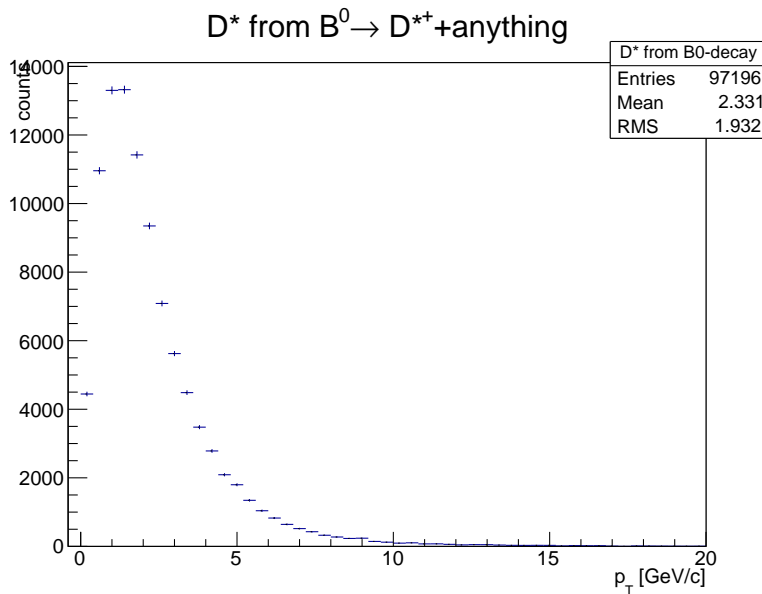

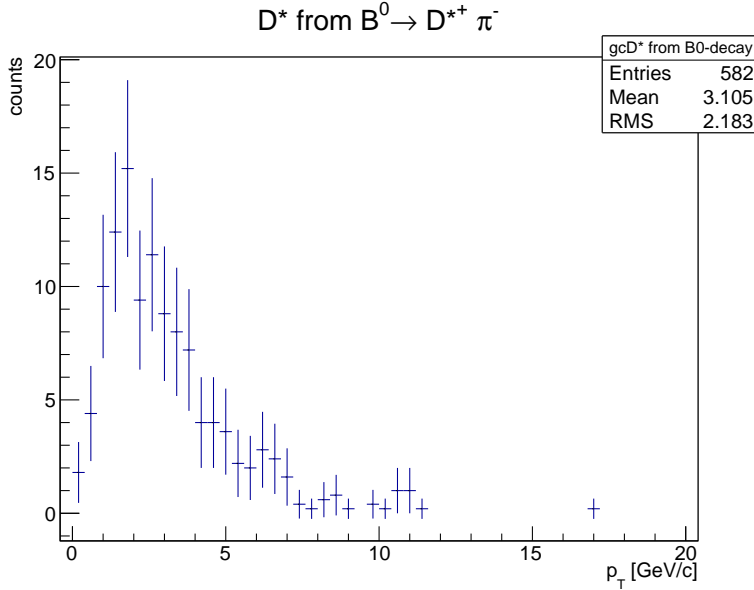Figure 30: p_T distribution for all D^{*+} we get in the events minus the ones from our prefered decays.

Figure 31: p_T distribution for all D^{*+} mesons coming from our preffered decay: $B^0 \rightarrow D^{*+}\pi^-$.

The most important thing here is that on average a D^{*+} from $B^0 \rightarrow D^{*+}\pi^-$ has a higher p_T then a D^{*+} coming from some other decay. With increased statistics we should see a distribution which has a relatively lower peak, which is spread out towards higher p_T. We could then create a division histogram, similar to figure 22, but as there are only 582 D^{*+} from $B^0 \rightarrow D^{*+}\pi^-$ the statistics are to low to present that histogram from this data.
Next we will look at the topology of the decay. The next plots are constructed by taking the direction in which the D^{*+} is flying and subtracting this by the direction of it's B^0 mother. This gives us the relative angle between the D^* flight line and the flight line of the B^0 flight line. This information can be used to improve our cutting criteria. There is a ϕ-plot and an η-plot. As the ALICE detector covers the full ϕ range, to study the acceptance the η-plot is more valuable.
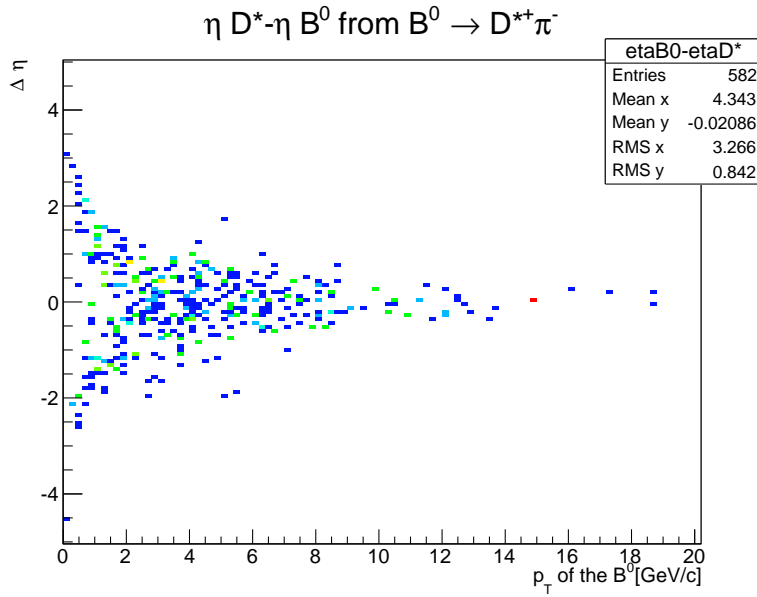
Figure 32: The angle in η for the D^{*+} when decaying from a B^0 in our preferred decay.
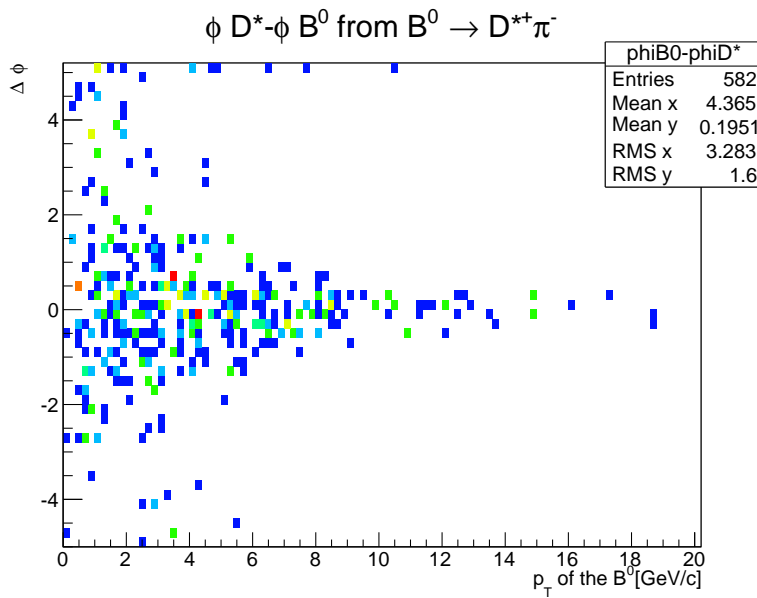

Figure 33: The angle in ϕ for the D^{*+} when decaying from a B^0 in our preferred decay.

Logically we see that at high energies the D^{*+} travels more in the direction

of its B^0 mother. But at low p_T the D^{*+} can travel in a completely different direction.

Further building on the acceptance study in p_T bins we take a look at figure 30 in p_T-slices. The next table shows the amount of D^{*+} in each bin and the amount that would be in acceptance if the mother B^0 travelled along the beam-axis ($\eta = 0$).

p_T range (Gev/c)	All D^{*+}	D^{*+} in acceptance	percentage in acceptance
0-2	157	56	35.8%
2-4	163	138	84.7%
4-6	118	107	91.5%
6-10	103	101	98.1%
10-16	37	37	100%
>16	4	4	100%

Note that these values do not include the initial flight line of the B^0. If we add these up, we get a total of 119 D^{*+} from our main channel that are in acceptance. Then offcourse we need two more decays. In our data this resulted in 4 pions and 3 kaons coming from a B^0 through our main channel, which would actually be viewable in ALICE. Taking in account the amount of events that will be produced in ALICE and the detector efficiency as in chapter 5.2.1, we should be able to see .... B^0 through the method described in section 3.3.

5.2.3 Secondary channel D^*

The downside of our main channel is obviously the lack of statistics. We have 582 D^{*+} from our main channel from 1.3 billion events (not even in minimum bias). From section 1.2 and figure 20 we can conclude this gives us approximately 15 D^0 that go into $D^0 \rightarrow K^-\pi^+$. That is where our secondary channel, $B^0 \rightarrow D^{*+} + e^+ + \nu_e$, shines. We get 10377 of these decays. Which is a factor of 20 more. The downside was described in section 5.1: the missing momentum of the neutrino gives us a larger uncertainty in the reconstruction of the invariant mass. So there are upsides and downsides, but it's a channel definately worth studying. We will start by looking at the p_T-distribution.
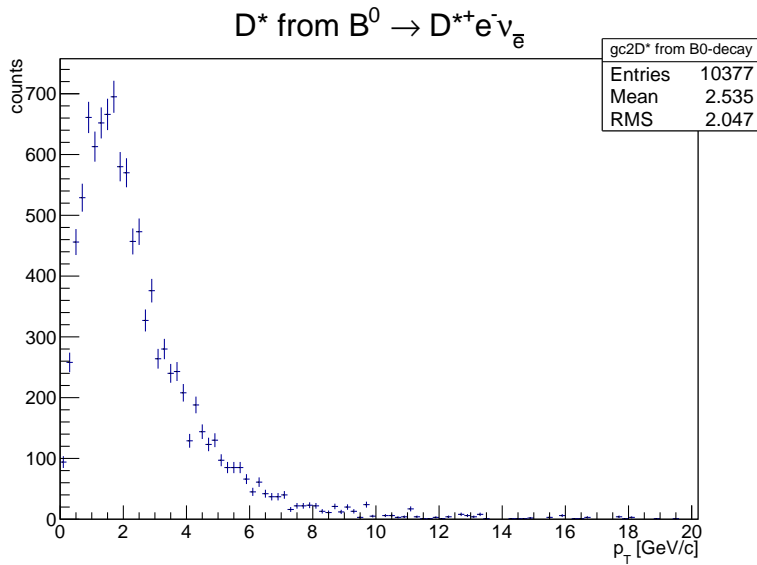
Figure 34: The p_T-distribution of the D^{*+} coming from our secondary channel.

We see that the average p_T is higher than the 'regular' D^{*+} (see figure 29), but not as high as in our main channel. Even though the average p_T is different, the higher statistics should give us a better picture of the topology of the decay.
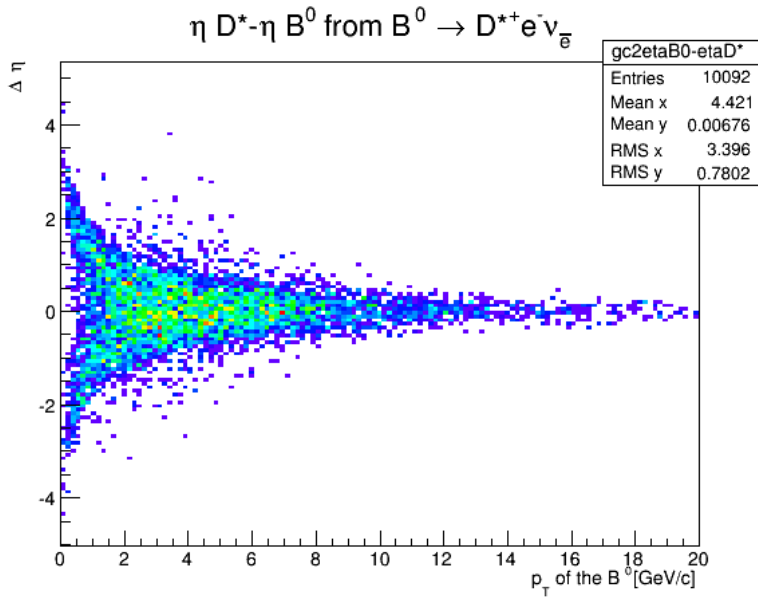
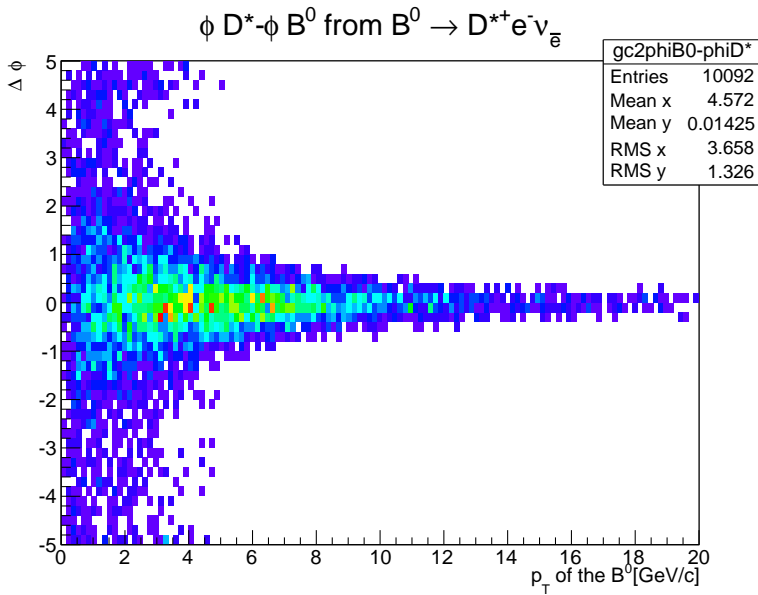Figure 35: The angle in η for D^{*+} mesons when decaying from a B^0 in our secondary channel.

Figure 36: The angle in ϕ for D^{*+} mesons when decaying from a B^0 in our secondary channel.

We can see the same problematic behaviour at low p_T.

6 Discussion

We started by looking at the data from p-p collisions in ALICE at 7 TeV from 2011. We searched for the D^{*+} and found good peaks in p_T the bins: 3-4, 4-5, 5-6, 6-8, 8-12, 12-16, 16-24, 24-36 GeV/c. The significance ranged from 3.7 to 7.9 with a total amount of 1525 D^{*+}. To examine the stability of the signal we extracted the yield using different fitting methods (see table below) and concluded that the signal is stable within 10%. We did the same for the particle identification (PID) from the TOF and the TPC and concluded that the signal is also stable within 10%. From this data we also tried to find the B^0, but we were unsuccesful. This is due to the poor statistics available.

p_T range (Gev/c)	Yield exctraction systematic (%)	PID systematic (%)
3-4	7	5
4-5	4	4
5-6	2	2
6-8	1	<1
8-12	1	2
12-16	7	2
16-24	5	7
24-36	9	4

This is why we turned to simulated data to study the B^0. Awaiting the upgrade of the accelerator at the LHC to 13 TeV, we predicted the possibilities to study the B^0 through our preffered decay channel. In 1.3 billion events, we found only 3 kaon-pion pairs that would be detectable in ALICE. Scaling for the amount of data that ALICE will produce (170 billion events) and the fact that we did not use a minimum bias model in our simulations; we expect to have 5771 $B^0 \rightarrow D^{*+}\pi^-$ in acceptance, which results in 151 $D^0 \rightarrow K^-\pi^+$ through the whole channel. We have also studied the acceptance in p_T bins, which gave us the following results:

p_T range (Gev/c)	In acceptance (%)	$B^0 \rightarrow D^{*+}\pi^-$ in ALICE in acceptance
0-2	5	1501
2-4	13	2109
4-6	18	1087
6-10	23	586
10-16	27	374
¿16	31	114

We see that $\sim 85\%$ of B^0 travel outside of our acceptance range (integrated over p_T) and that at low p_T we lose a lot more than at high p_T. When studying the kinematics of the D^{*+} coming from B^0 we made two main conclusions. We saw that relative to the B^0 flight line, the D^* daughter decays in very high angles at low p_T. In comparing the D^{*+} from our main channel to 'regular' D^{*+} we concluded that the ones from our main channel are signifanctly harder. In examining our secondary channel, we concluded that we get approximately 20 times more B^0. Despite the problems in reconstructing the neutrino momentum, this might be a promising channel to study the B^0.

REFERENCES

[1] K. Nakamura *et al.* (Particle Data Group). *Review of Particle Physics.* J. Phys. G: Nucl. Part. Phys. 37 (2010) 075021.

[2] A. Grelli. *Heavy Flavour Physics with the ALICE detector at the CERN-LHC.* Approved for publication (2011).

[3] R.S. De Rooij *Prompt D*+ production in proton-proton and lead-lead collisions, measured with the ALICE experiment at the CERN Large Hadron Collider.* Dissertation, Utrecht Unversity (2013).

[4] http://aliceinfo.cern.ch/

Acknowledgements

I would like to thank my supervisors A. Mischke and A. Grelli. Without their guidance I would not have had much to write about. I realise that I can be chaotic and absent-minded, but I've always received patience and advice in return. For which my thanks. I hope that in this process I have given something back, however small that may be compared to what I have received.